Capillary-Marangoni Synergism Enabled Salt-Resisting Sodium Alginate Hydrogel Foam for Efficient Solar-Driven Water Harvesting

Yong Li,[a*] Deyun Yue,[a] Minqi Cui,[a] Danning Cao,[a] Mengyao Wang,[a] Haojie Song[a*]

[a] School of Materials Science & Engineering, Key Laboratory of Underground Cultural Relics Conservation Materials and Technology, Ministry of Education, Shaanxi University of Science & Technology, Xi' an, 710021, PR China

[*] Corresponding author.
E-mail address: yongli@sust.edu.cn; songhaojie@sust.edu.cn

1. Supporting Note

Note S1 Configuration of heavy metal ion solution and simulated seawater

The composition of simulated seawater consists mainly of sodium chloride, magnesium sulfate, calcium chloride, potassium chloride, potassium bromide and other trace elements. Usually, the concentrations of Ca^{2+}, Mg^{2+}, Na^{+} and K^{+} ions are 410 mg/L, 1310 mg/L, 10900 mg/L and 390 mg/L. A certain amount of calcium chloride, magnesium sulfate, sodium chloride, and potassium bromide are used in deionized water until they are completely dissolved.

This experiment mainly tested four common metal ion pollution, Cu^{2+}, Fe^{3+}, Co^{2+} and Zn^{2+}, and the concentration of the four metal ions was 300mg/L. After calculation, a certain amount of $FeCl_3 \cdot 6H_2O$, $Co(NO_3)_3$, $Cu(NO_3)_2 \cdot 3H_2O$ and $Zn(NO_3)_2$ were put in deionized water until completely dissolved.

Note S2 Water evaporation efficiency calculations.

The efficiency calculation formula is defined as:

$$\eta = \frac{(m_0 - m_1)h_{LV}}{C_{opt}P_0} \quad (1)$$

Where, η is the water evaporation efficiency of SA-PPy@MF at sunlight; m_0 is the water evaporation rate of SA-PPy@MF under light (kg m^{-2} h^{-1}); m_1 is the water evaporation rate of SA-PPy@MF Under without light conditions (kg m^{-2} h^{-1}); h_{LV} is the enthalpy of water vaporization; C_{opt} is the optical intensity, P_0 is the standard solar radiation (1 kW m^{-2}).

Table S1 Evaporation rate and efficiency of different hydrogels.

Evaporator	v/(kg m^{-2} h^{-1})	η/%	Evaluate
Ag-Pss-AG/AG[1]	2.10	92.8	Efficient water transport capacity. Stability and practicality. The preparation process is relatively complex.
Cu@C/CLS[2]	1.54	90.2	Excellent 3D porous structure. Excellent stability. Complex preparation process.
Au nanoturf[3]	1.13	91	Efficient macro-nano thermal insulation. Self-powered system. Gold nanoflowers may agglomerate or degrade.
HNG[4]	3.2	94	Excellent 3D porous structure. Excellent stability. Complex preparation process.
PPyP[5]	2.99	85.89	Can switch between 2D and 3D structures. Excellent mechanical strength. Long-term performance degradation.
P-CHG[6]	3.02	89.09	Strong salt resistance. Good thermal insulation effect. Removal efficiency for different types of pollutants.
PANI-SPPSU@PU[7]	1.91	83.59	Excellent salt tolerance. Material degradation issues. Easy preparation and scalability.
PPy-A[8]	2.03	93.3	Excellent light absorption properties. Efficient photothermal conversion. Salt crystallization issues.
Bamboo[9]	3.13	132	3D structure effectively enhances evaporation efficiency. Raw materials are environmentally friendly. Temperature sensitivity may lead to degradation of carbonized bamboo in high-temperature environments.
F-wood[10]	3.46	81	Good hydrophilicity.

HCT@PC[11]	1.86	95.86	Low thermal conductivity. Potential limitations in raw material availability. Excellent photothermal conversion and evaporation performance. Environmentally friendly.
SA-PPy-800@MF (This work)	3.47	95	Complex preparation process. Superior capillary force. A photothermal layer with efficient thermal management capabilities. Excellent stability and strong salt-rejection resistance.

2. Supporting Figures

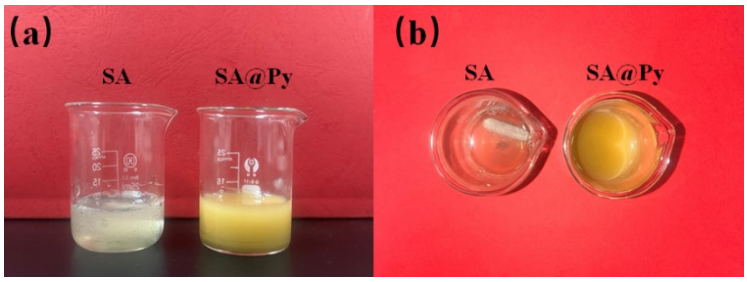

Fig. S1 (a, b) Photographs of sodium alginate and SA-Py solution after uniform stirring.

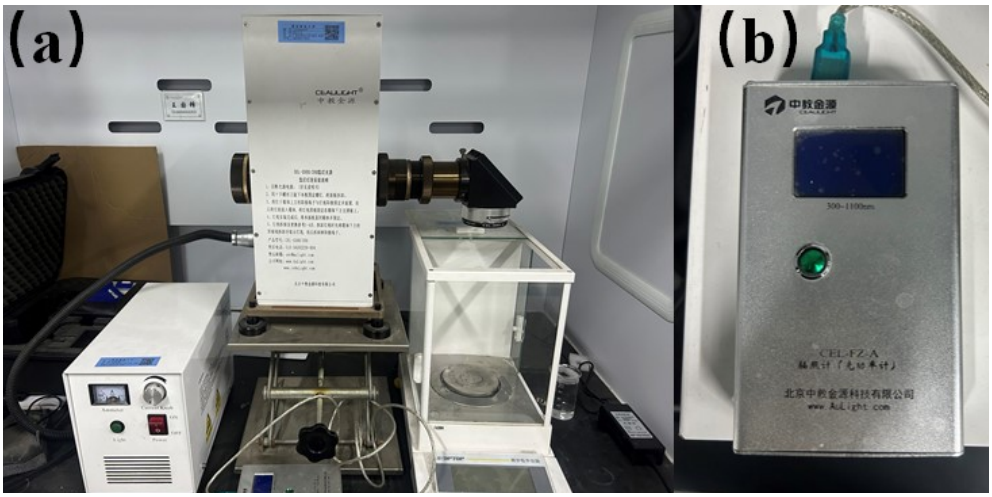

Fig. S2 (a) Solar simulator as the light source. (b) CEL-FZ-A optical power meter.

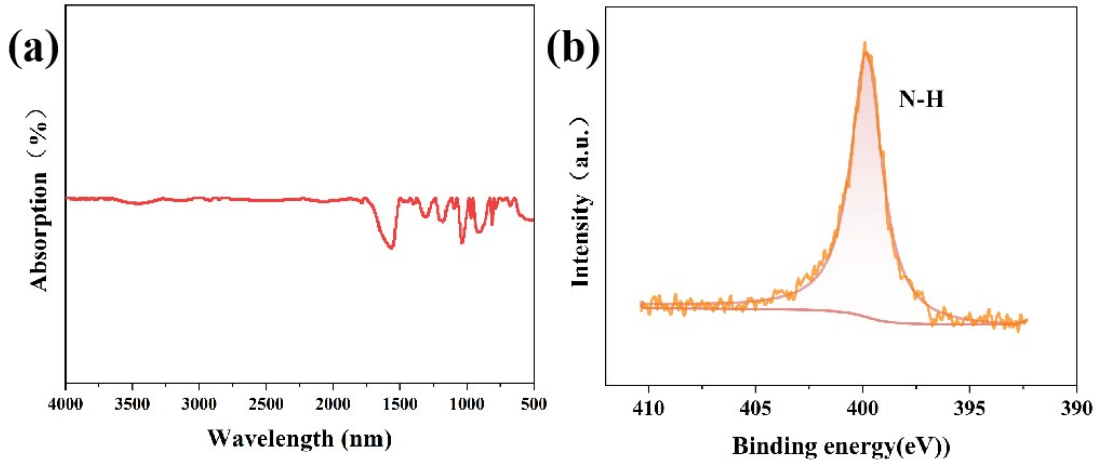

Fig S3 (a) Fourier transform infrared spectroscopy (FT-IR) of SA-PPy@MF. (b)High-resolution N 1s spectrum of the SA-PPy@MF solar absorber.

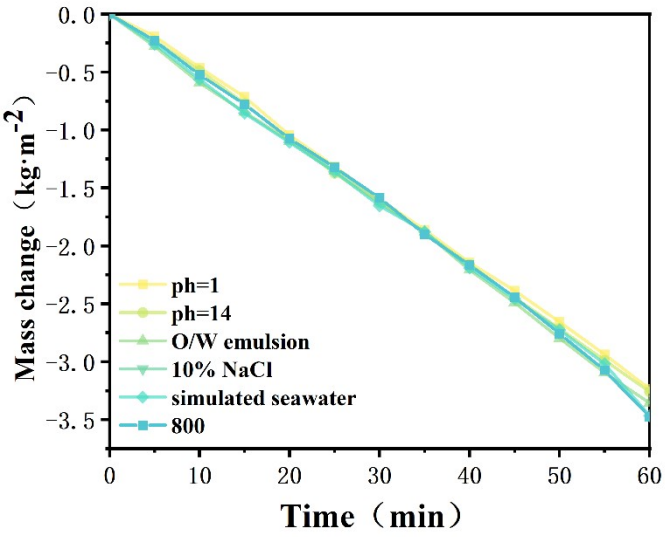

Fig. S4 Mass change and evaporation rate of SA-PPy-800@MF in different solution environments under 1 sun.

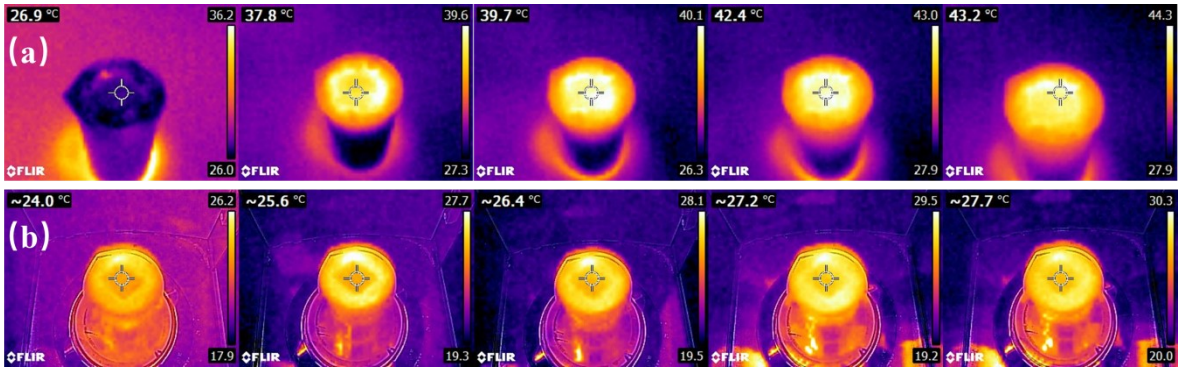

Fig. S5 (a) Temporal variation of the SA-PPy@MF surface temperature under 1 sun illumination, recorded at 0, 5, 10, 30, and 60 min. (b) Temporal variation of the pure water surface temperature under 1 sun illumination, recorded at 0, 5, 10, 30, and 60 min.

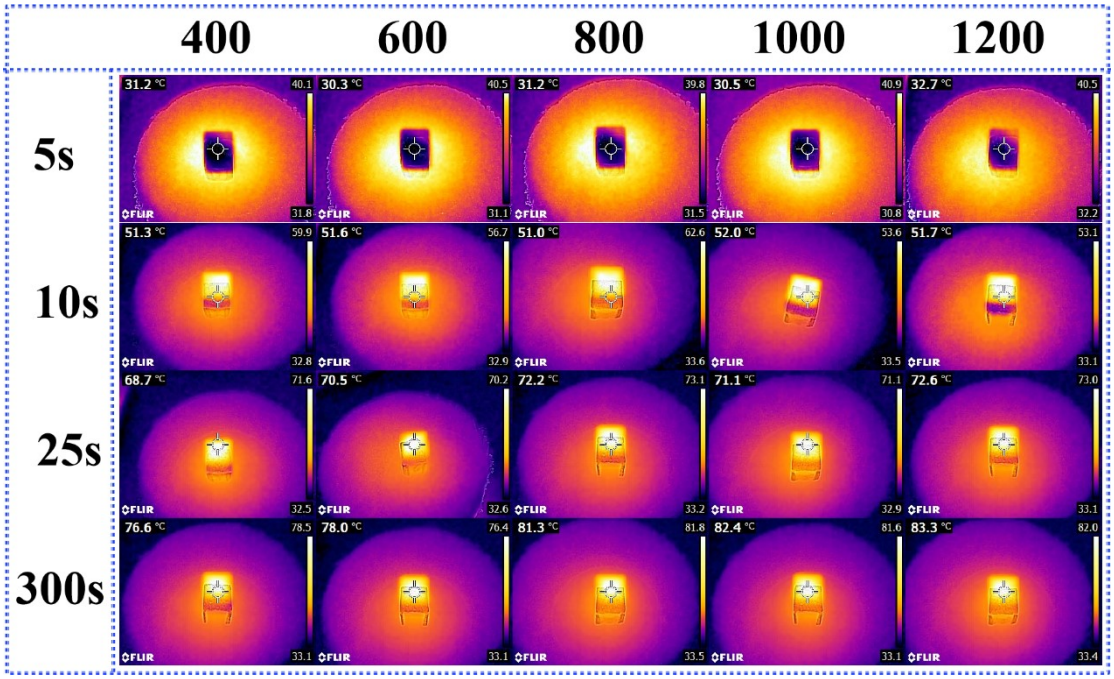

Fig. S6 Top surface temperatures of dry SA-PPy@MF aerogels under 1 sun.

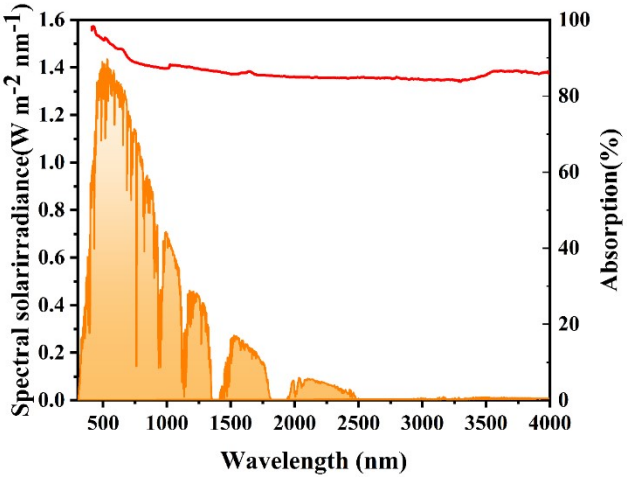

Fig. S7 UV-vis-NIR absorption spectra of the SA-PPy-800@MF aerogel (200-2500 nm).

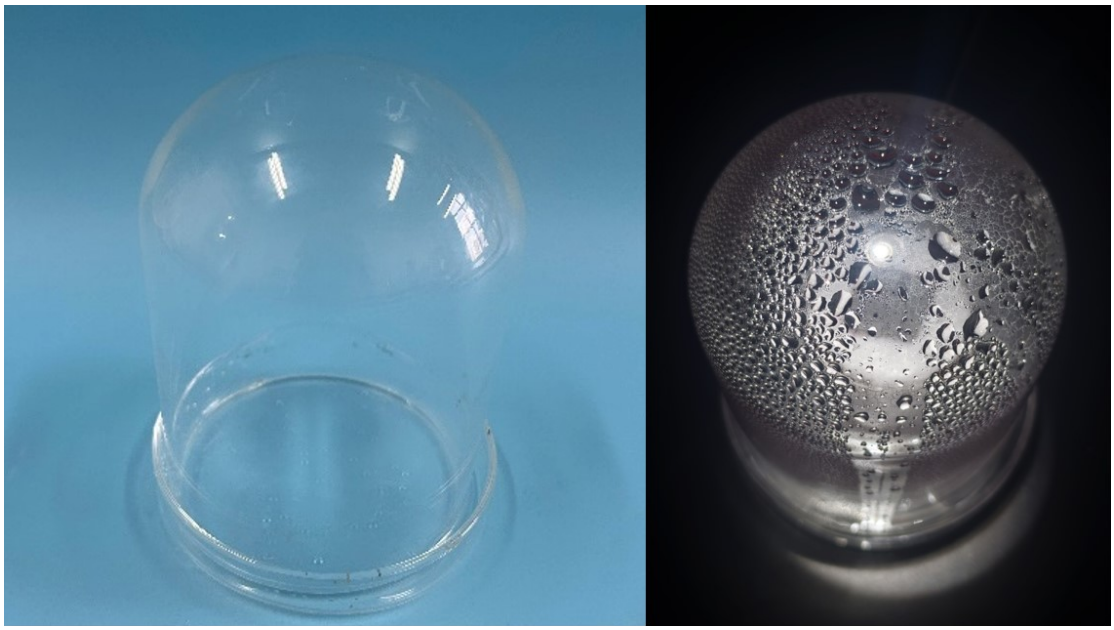

Fig. S8 Condensate collection device.

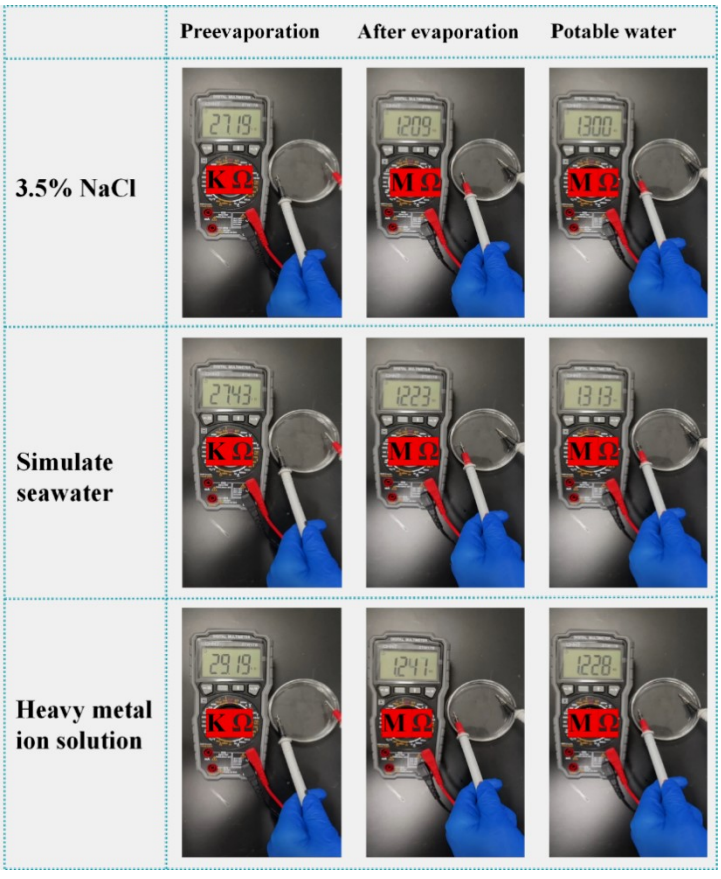

Fig. S9 Multimeter measurement of water sample purity (from left to right; units: kΩ, MΩ, MΩ).

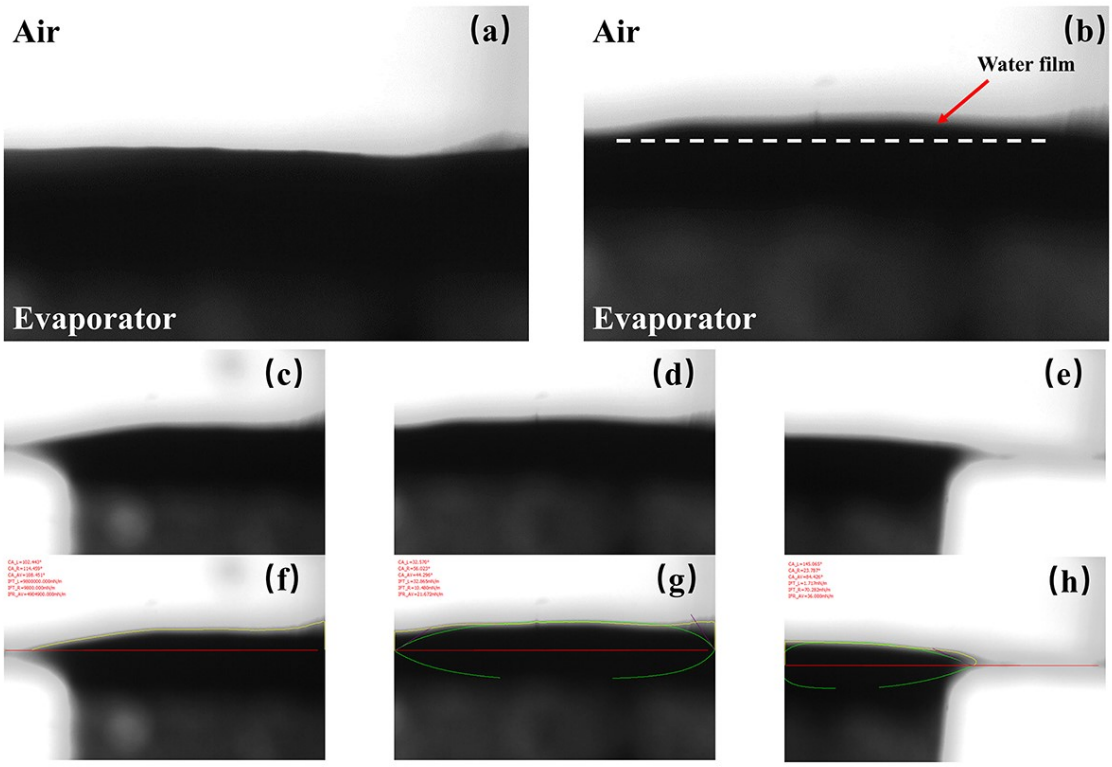

Fig. S10 Photographic images of the air-water evaporator interface at (a) 0 min and (b) 30 min. (c-e) Images corresponding to the left, middle, and right sections of the evaporator, respectively. (f-h) Corresponding fitted contact angle data.

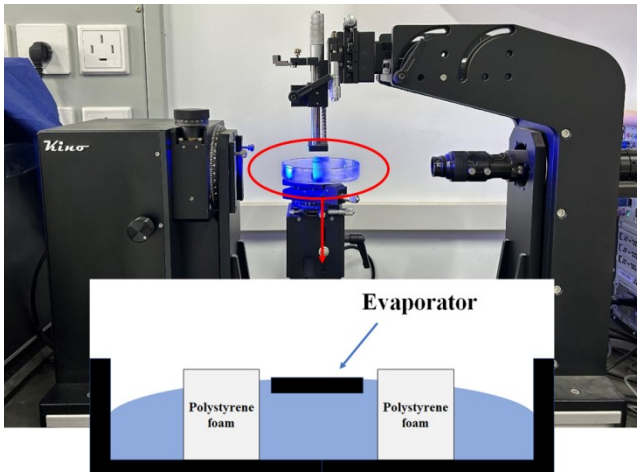

Fig. S11 Contact angle measurement and water film test device.

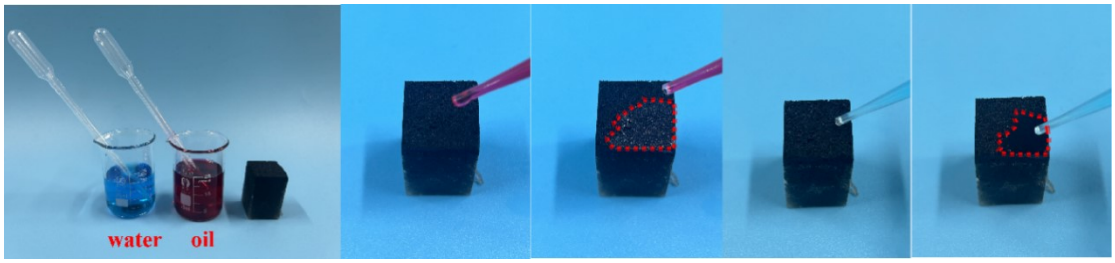

Fig. S12 Oil and water wettability of SA-PPy-800@MF in air.

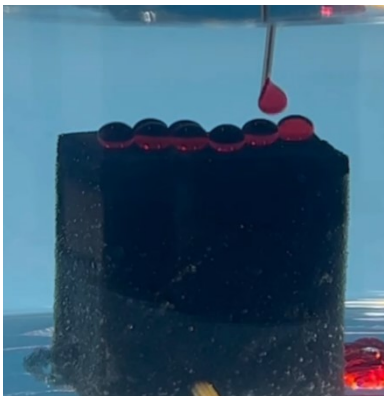

Fig. S13 Photograph of oil drops on the surface of SA-PPy-800@MF under water.

Fig. S14 Underwater oil drop contact angle on the SA-PPy-800@MF surface.

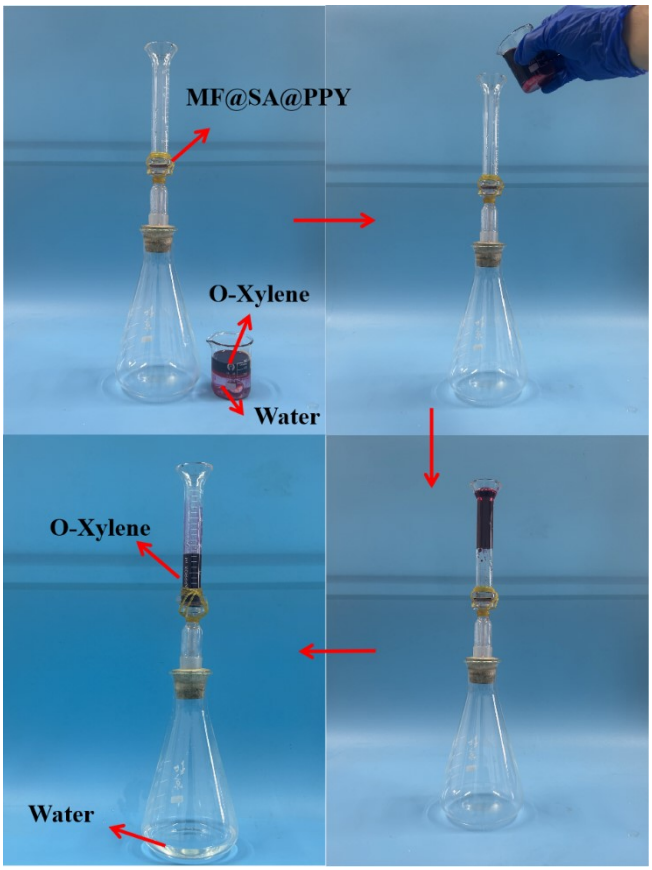

Fig. S15 Photographs of oil-water mixture separation using SA-PPy-800@MF.

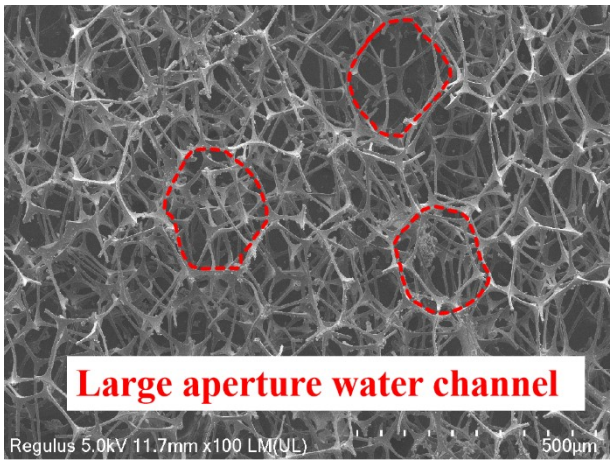

Fig. S16 Large aperture water channel.

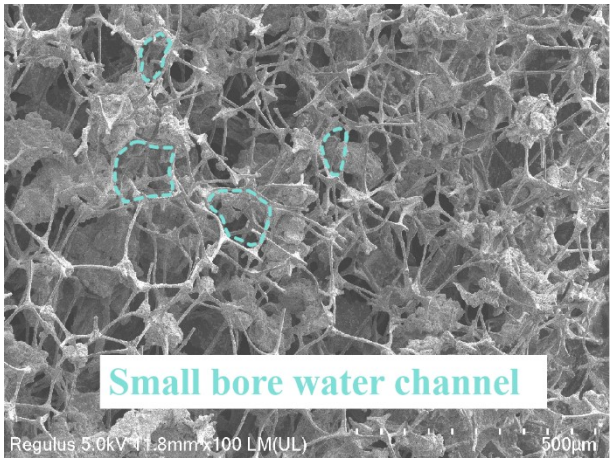

Fig. S17 Small bore water channel.

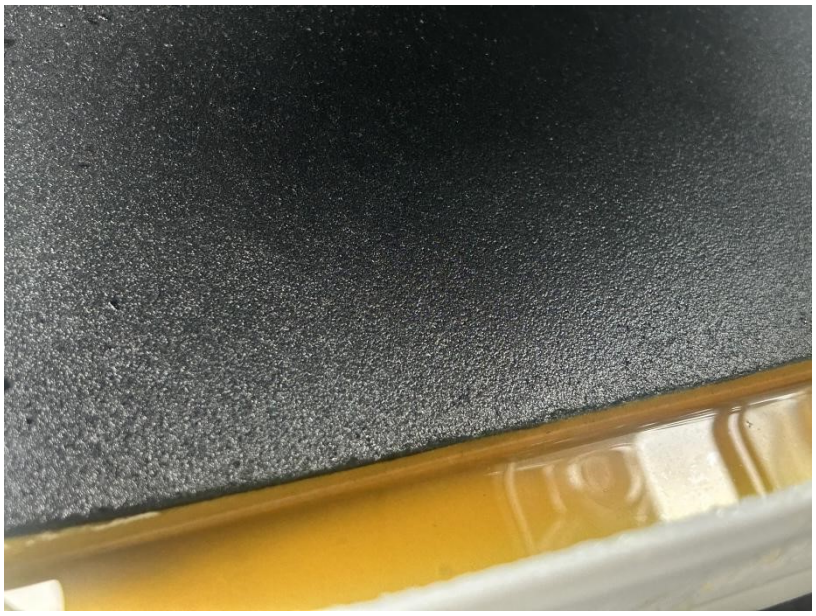

Fig. S18 Photograph of the 30 × 30 cm SA-PPy-800@MF evaporator.

Fig. S19 Top view of the SA-PPy-800@MF evaporator.

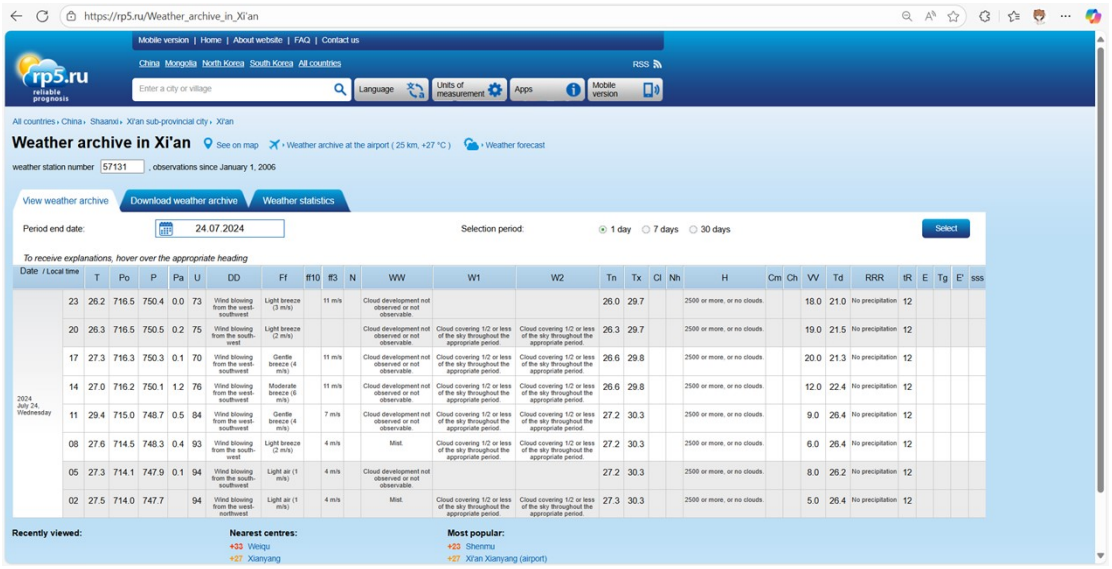

Fig. S20 Field tests conducted on July 25-26, 2024, at Shaanxi University of Science and Technology, China, evaluated the evaporator's performance under real-world weather conditions, including wind speed, solar irradiation, and ambient temperature.

Fig. S21 Stress test of the SA-PPy-800@MF evaporator.

Fig. S22 Bending test of the SA-PPy-800@MF evaporator.

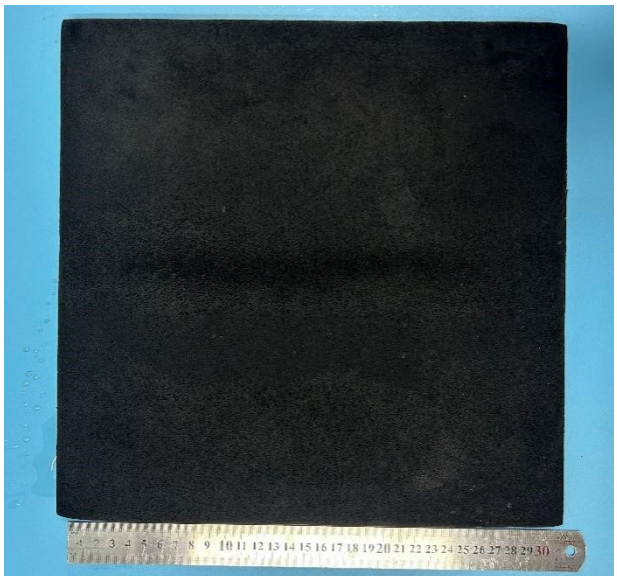

Fig. S23 Recovery of the original state of the SA-PPy-800@MF evaporator after compression-release.

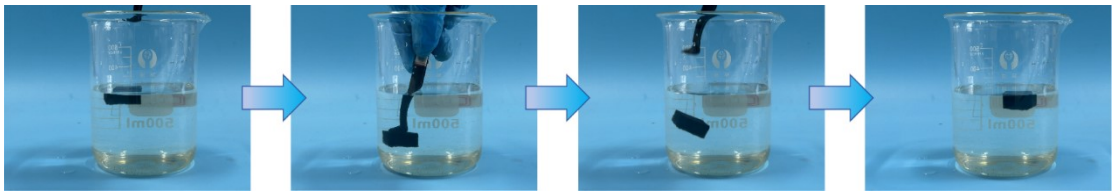

Fig. S24 Self-flotation test of the SA-PPy-800@MF evaporator.

References

1 Z. Sun, J. Wang, Q. Wu, Z. Wang, Z. Wang, J. Sun and C. Liu, *Adv. Funct. Mater.*, 2019, **29.29**, 1901312.

2 L. Ren, X. Yi, Z. Yang, D. Wang, L. Liu and J. Ye, *Nano Lett.*, 2021, **21.4**, 1709-1715.

3 M. Gao, C. Peh, H. Phan, L. Zhu and G. Ho, *Adv. Energy Mater.*, 2018, **8.25**, 1800711.

4 F. Zhao, X. Y. Zhou, Y. Shi, X. Qian, M. Alexander, X. P. Zhao, S, Mebdez, R. G. Yang, L. T. Qu and G. H. Yu, *Nat. Nanotechnol.*, 2018, **13.6**, 489-495.

5 F. Ni, P. Xiao, C. Zhang, Y. Liang, J. C. Gu, L. Zhang and T. Chen, *ACS Appl. Mater. Interfaces*, 2019, **11.17**, 15498-15506.

6 L. Shu, X. F. Zhang, Z. G. Wang, J. Liu and J. F. Yao, *Carbohydr. Polym.*, 2024, **327**, 121695.

7 X. T. Zhao, J. J. Dong, X. H. Yu, L. L. Liu, J. L. Liu and J. F. Pan, *Sep. Purif. Technol.*, 2023, **311**, 123181.

8 C. Gao, Y. M. Li, L. Z. Lan, Q. Wang, B. G. Zhou, Y. Chen, J. C. Li, J. S. Guo and J. F. Mao, *Adv. Sci.*, 2024, **11.6**, 2306833.

9 Y. Bina, Q. Q. Du, K. Tang, Y. Shen, L. C. Hao, D. Zhou, X. K. Wang, Z. H. Xu, H. L. Zhang, L. J. Zhao, S. M. Zhu, J. D. Ye, H. Lu, Y. Yang, R. Zhang, Y. D. Zheng and S. L. Gu, *Adv. Mater. Technol., 2019*, **4.4**, 1800593.

10 G. B. Xue, K. Liu, Q. Chen, P. H. Yang, J. Li, T. P. Ding, J. J. Duan, B. Qi and J. Zhou, *ACS Appl. Mater. Interfaces*, 2017, **9.17**, 15052-15057.

11 J. Wu, X. Y. Yang, X. H. Jia, J. Yang, X. Miao, D. Shao, H. J and Song, Y. Li, *Chem. Eng. J.*, 2023, **471**, 144684.